Disorder-type-dependent phase diagram in a CsCl-type complex Anderson lattice model

Limin Wang and Weiyi Zhang
Nanjing National Laboratory of Microstructures and Department of Physics, Nanjing University, Nanjing 210093, China
(Received 11 October 2009; revised manuscript received 28 December 2009; published 3 February 2010)

The investigation on disorder-driven metal-insulator transition of the Anderson lattice model has been extended to a CsCl-type complex lattice to accommodate for the hybridized bands originating from atomic orbitals of inequivalent lattice sites. Using the standard transfer-matrix method and finite-size scaling an asymmetrical mobility edge is found in the energy-disorder phase diagram under site-selective disorder. The critical disorder is larger in the less disorder-affected band than its counterpart in the more disorder-affected band. Moreover, a unique type of delocalized state appears at the edge of the less disorder-affected band. The asymptotic localization length $\lambda_M(W)$ increases linearly with the longitudinal sample size, which depends neither on the lateral size M nor on the disorder strength W. Except for this particular energy, metal-insulator transitions exist for all other energies and reduced localization lengths satisfy the single-parameter scaling law. The critical exponent, $\nu \approx 1.5-1.6$, is in good agreement with the previous results. The critical disorder is larger than that of a simple cubic lattice due to increased coordination number. The complex Anderson lattice model considered here has the advantage of simulating the localization disparity between electron- and hole-doped bands in the presence of site-selective disorder.

DOI: 10.1103/PhysRevB.81.054204 PACS number(s): 72.15.Rn, 72.20.Ee

I. INTRODUCTION

The metal-insulator transition (MIT) in disordered systems has been the subject of theoretical[1–15] and experimental studies[16–19] since the pioneering work by Anderson in his famous paper[1] nearly 50 years ago. In the absence of electronic interaction and external magnetic field, the single-parameter scaling theory,[2,3] supplemented by the weak localization theory,[4] predicts that an MIT exists only in three-dimensional (3D) systems.[3] The delocalized or extended states exist when the disorder is relatively weak while the strong disorder favors localized states due to the interference of electron wave function with itself. Various numerical approaches,[5] such as the transfer-matrix method (TMM),[6–8] the recursive Green's function method,[9–13] the energy-level statistics,[14] and the multifractal analysis,[15] have been used to simulate the localization behaviors in these systems, and most of them support the conclusion of the single-parameter scaling theory that a disorder-driven metal-insulator transition takes place only in 3D systems.

Among the lattice type studied so far, the simple cubic (SC) lattice is the most extensively studied case of 3D disordered electronic systems. For uniform diagonal disorder, the critical exponent and critical disorder at the band center ($E=0$) have been calculated by several groups.[8,20] The best values are estimated to be $\nu=1.57\pm0.02$ (Ref. 20) and $W_C=16.54\pm0.02$.[8,20] Further studies suggested that the critical exponent obtained at the band center is quite universal and truly representative of the whole band. The metal-insulator phase diagram in the energy-disorder phase space shows a symmetrical pattern with respect to the band center. The critical disorder W_C is nearly independent of the energy[5,12] if the energy is within the unperturbed band. For energy outside the unperturbed band, the reentrance phenomenon takes place due to the competition between quantum interference and disorder-driven band broadening. In contrast to the conclusion reached above for diagonal disordered systems, the off-diagonal disorder is generally unable to localize all states in the system.[21–23] The extended states always exist close to the band center irrespective of the disorder strength. In addition to the simple cubic lattice, the localization behaviors in more compact body-centered cubic (BCC) and face-centered cubic lattices have been investigated recently by Eilmes *et al.*[24] The critical exponents are essentially the same among the three different types of lattices of the same universality class and the value of critical disorder W_C increases with the coordination number of lattice types.[24]

However, in many mixed valence semiconductors or doped perovskites, the primary cell usually contains more than one type of atom. The electronic bands near the Fermi energy are composed of valence and conduction bands resulting from hybridization among the neighboring atoms of different types. On the one hand, a doped atom favors one atomic site over the other, thus the doping-induced disorder is not evenly distributed among different atomic sites; on the other hand, electron doping and hole doping move the Fermi energy either to conduction band or to valence hand. As a result, the localization property and the phase diagram become asymmetrical with respect to the carrier type of doping. The single-band Anderson lattice models are clearly unable to address this issue and the many-band complex Anderson lattice models are called for. It should be emphasized that the binary disorder model[25] simulates the alloy property very well and also leads to two separate bands but the spectral weight of each band is composition dependent which distinguishes itself from two-band lattice models. Since the scaling behavior and localization property of many-band lattice model are largely unknown, we have considered in this paper a simplified two-band lattice model in three dimension (Fig. 1). Though we consider only the diagonal disorder in the present model, the effective one-band lattice model for either sublattice always includes off-diagonal disorder as well as diagonal disorder. Therefore, our complex lattice model also serves as a bridge connecting the diagonal and the off-diagonal disorders. Furthermore, the

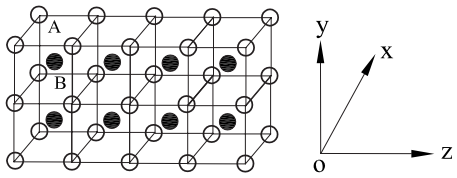

FIG. 1. Schematic of the complex Anderson lattice. *A* and *B* sites form two simple cubic lattices embedded at each other's center. The propagation direction is along the *z* axis, and lateral directions are denoted by the *x* and *y* axes.

site-selective disorder in the present model may offer useful insight on the carrier-type-dependent localization property in high-T_C superconductors and other transition-metal oxides.

Thus, we have performed in this study a high-precision computation on the localization lengths using the standard transfer-matrix method and analyzed the property of this complex Anderson lattice model using finite-size scaling. To check the numerical accuracy we first reproduce the localization lengths and critical behavior of the BCC lattice model, and excellent agreement is reached with the recent study.[24] For the two-band case with either uniform disorder or site-selective disorder, the critical exponent remains roughly the same as that of one band. The phase diagram can be quite different depending on the disorder type. A mirror reflection symmetry exists among the two bands if the uniform disorder is applied but such symmetry is destroyed under site-selective disorder. Furthermore, the critical disorder is different for the conduction and valence bands in the case of site-selective disorder. The disorder tends to localize more easily the states in the band whose atomic orbitals are most affected. One interesting feature is the delocalized state at the lower edge of less disorder-affected band. The asymptotic localization length $\lambda_M(W)$ increases linearly with the sample size up to the largest layer number $L=2\times10^9$ the computer can handle. It is six orders of magnitude larger than the lateral size M and depends neither on the lateral size M nor on the strength of disorder W.

The rest of the paper is organized in the following way. In Sec. II, we first introduce the lattice model under consideration. The standard transfer-matrix method is then briefly described and the finite-size scaling is outlined. The localization lengths, scaling properties, and phase diagrams for typical cases are presented in Sec. III. These data are discussed and compared with previous results. Finally, a summary is given in Sec. IV.

II. MODELS AND METHODS

The complex lattice model we considered in this paper consists of two superimposed cubic lattices on each other's body center, as shown in Fig. 1. The propagational direction of the wave function is taken along the *z* axis while the periodic boundary condition is imposed in the *x* and *y* axes. The tight-binding Hamiltonian in site representation is

$$H=\sum_{i\in A}|i\rangle\epsilon_i^A\langle i|+\sum_{j\in B}|j\rangle\epsilon_j^B\langle j|+\sum_{i\in A,j\in B}[t_{ij}|i\rangle\langle j|+\text{H.c.}], \tag{1}$$

where $\epsilon_i^A=-0.5\Delta+w_i$ and $\epsilon_j^B=+0.5\Delta+w_j$ are, respectively, the on-site energies in the *A* and *B* sublattices with Δ denoting charge-transfer energy between the two sublattices, and w_i and w_j are random numbers simulating the diagonal disorder. Only the nearest-neighbor hopping-matrix element is considered and set to be 1 as the energy scale. The random numbers w_i and w_j are assumed to take a uniform distribution in the intervals $[-W_A/2,W_A/2]$ and $[-W_B/2,W_B/2]$, where W_A and W_B are the disorder strengths in the two sublattices.

In the case of $\Delta=0$ and $W_A=W_B=W$, the two sublattices become indistinguishable and the lattice structure reduces to that in the BCC lattice.[24] In the absence of disorder, the unperturbed band structure is given by $E(\vec{k})=8\cos(k_x/2)\cos(k_y/2)\cos(k_z/2)$. The density of states (DOS) is symmetrical with respect to the band center and extends from −8 to +8. Note that there is a logarithmic singularity in the density of states at $E=0$.[26]

When charge-transfer energy is finite, the *A* and *B* sublattices become distinguishable. The primary cell is doubled and two unperturbed electronic bands read $E(\vec{k})=\pm\sqrt{[0.5\Delta]^2+[8\cos(k_x/2)\cos(k_y/2)\cos(k_z/2)]^2}$. The densities of states have a mirror reflection with respect to $E=0$. The lower band is dominated by the orbitals of *A* sites and spans from $-\sqrt{8^2+[0.5\Delta]^2}$ to -0.5Δ while upper band is dominated by the orbitals of *B* sites and spans from $+0.5\Delta$ to $+\sqrt{8^2+[0.5\Delta]^2}$. Each band has a band width $\sqrt{8^2+[0.5\Delta]^2}-0.5\Delta$. In particular, the original logarithmic singularity in the density of states at $E=0$ for the simple BCC lattice gets split and diverges in the form $N(E)\propto\frac{1}{\sqrt{E^2-(\Delta/2)^2}}\ln\frac{\Delta}{\sqrt{E^2-(\Delta/2)^2}}$ at the edges $E=\pm\Delta/2$.

Although we include only the diagonal disorder here for our complex lattice, the disorder effect on each band, in fact, involves both diagonal as well as off-diagonal disorders. This can be most easily seen if we integrate out the orbital degrees of freedom of one sublattice and concentrate on the band dominated by the orbitals of other sublattice. In the simplified case where t/Δ can be treated as a small parameter, the effective Hamiltonian for the *A* sublattice can be obtained within the second-order perturbation[27,28]

$$H_{eff}^A=\sum_{i\in A}\left[\epsilon_i^A+\sum_{j\in B}\frac{t_{ij}t_{ji}}{\epsilon_i^A-\epsilon_j^B}\right]|i\rangle\langle i|+\sum_{i,i'\in A}\sum_{j\in B}\left[\frac{t_{ij}t_{ji'}}{\epsilon_i^A-\epsilon_j^B}+\frac{t_{i'j}t_{ji}}{\epsilon_{i'}^A-\epsilon_j^B}\right]|i\rangle\langle i'|. \tag{2}$$

Similar expression can be obtained for *B* sublattice by index exchange $i\leftrightarrow j$ and $A\leftrightarrow B$. The reduced Hamiltonian shows that both the on-site energies and hopping-matrix elements are renormalized and disorder dependent.

To extract the localization length of the complex lattice model, we consider a finite lattice of L layers with $M\times M$ sites in cross section. The tight-binding Schrödinger equations of Hamiltonian (1) can be expressed as

$$C_{AB}\psi(l+1)=[EI-H_A(l)]\psi(l)-C_{AB}\psi(l-1) \tag{3}$$

with l layer standing for the *A* sublattice in neighboring with two layers of *B* sublattice. The equation for a layer of *B* sublattice in neighboring with two layers of *A* sublattice can be similarly derived by interchange $l\leftrightarrow l+1$ and $A\leftrightarrow B$. E is

the electron energy at which the localization property is to be investigated and $\psi(l)$ is the tight-binding wave function in lth layer with $M \times M$ components. I is a unit matrix, and $H_A(l)$ and $H_B(l)$ are Hamiltonian matrices representing the on-site energies in the A and B sublattices. The C_{AB} and C_{BA} are, respectively, the hopping matrices from the A layer to the B layer and vice versa, which are given by the following expression:

$$C_{AB} = C_{BA}^{tr} = \begin{pmatrix} D & D & & & & & \\ & D & D & & & & \\ & & \ddots & & & & \\ & & & D & D & & \\ & & & & \ddots & & \\ D & & & & & & D \end{pmatrix},$$

$$D = \begin{pmatrix} 1 & 1 & & & & & \\ & 1 & 1 & & & & \\ & & \ddots & & & & \\ & & & 1 & 1 & & \\ & & & & \ddots & & \\ 1 & & & & & & 1 \end{pmatrix}. \quad (4)$$

The recursive relation of Eq. (3) can be further cast into a transfer-matrix form after multiplying it by C_{AB}^{-1}

$$\begin{bmatrix} \psi(l+1) \\ \psi(l) \end{bmatrix} = \begin{bmatrix} C_{AB}^{-1}E - C_{AB}^{-1}H_A(l) & -I \\ I & 0 \end{bmatrix} \begin{bmatrix} \psi(l) \\ \psi(l-1) \end{bmatrix} = T_l \begin{bmatrix} \psi(l) \\ \psi(l-1) \end{bmatrix} \quad (5)$$

and a similar equation relating layer of the B sublattice with layers of the A sublattice also holds. Here, T_l is the usual transfer matrix. Thus, for given initial values of wave functions in the first and second layers, the calculation of electronic propagation along a quasi-one-dimensional bar is equivalent to compute the resultant transfer matrix for a specified layer number L, $G_L = \prod_{l=1}^{L} T_l$. In the thermodynamical limit, $G_\infty = \lim_{L\to\infty}(G_L G_L^+)^{1/2L}$ approaches a limiting matrix according to Oseledec's theorem.[29] Thus the electronic states and their localization properties are encoded in the eigenvalues and corresponding eigenfunctions in the limiting matrix. G_L is a symplectic matrix, and its eigenvalues appear in pairs with the form ($e^{-\gamma_m(W)}$ and $e^{+\gamma_m(W)}$). $\gamma_m(W)(>0)$s are Lyapunov exponents and their inverses $1/\gamma_m(W)$ describe the characteristic length scales of their wave functions. The largest length identifies the weakest possible decay of transmission probability along the propagation direction so localization length is defined as the smallest of them[5,10]

$$\lambda_M(W) = \frac{1}{Min_{m=1,2,\ldots,M^2}[\gamma_m(W)]}. \quad (6)$$

To achieve required numerical accuracy, a huge number of layers are needed to have the statistical error under control. To safeguard the information on the smallest eigenvalue, a systematic orthogonalization procedure is carried out during matrix multiplications.[10] The accuracy of $\lambda_M(W)$ is derived from the variance of the smallest Lyapunov exponent in the course of iteration.

Since the computed data of $\lambda_M(W)$ usually cover only a relatively small M, finite-size scaling has to be applied to extract the localization length for the system with an infinite cross section. This is conducted by treating $\Lambda_M(W) = \lambda_M(W)/M$ as a proper scaling variable and by fitting all curves with different W into a common scaling function[10]

$$\Lambda_M(W) = \frac{\lambda_M(W)}{M} = f\left[\frac{\xi(W)}{M}\right]. \quad (7)$$

Once the scaling parameter $\xi(W)$ is available, one can expand the quantity around the critical disorder, $\xi(W) = c|W - W_C|^{-\nu}$, to determine the critical exponent ν and critical disorder W_C.

However, the above procedure has difficulty to achieve high-precision scaling parameters since the divergence of $\xi(W)$ at W_C is rounded due to the limited $\Lambda_M(W)$ accuracy at critical point.[20,24] To address this issue, a new method[20,24] has been devised which accounts for the drifting of cross point due to finite size and nonlinearity of $\xi(W)$ away from critical disorder. A better numerical accuracy is achieved by fitting directly the raw data from TMM calculations to a generalized scaling function

$$\Lambda_M(W) = F[\chi_r(W)M^{1/\nu}, \chi_i(W)M^y], \quad (8)$$

where $\chi_r(W)$ denotes the relevant scaling variable describing the nonlinearity of scaling parameter and $\chi_i(W)$ stands for the irrelevant scaling variable describing the drifting of cross point due to finite size. ν and $y<0$ are the critical exponent and irrelevant exponent, respectively. F is then Taylor expanded up to order n_i in terms of the second argument

$$\Lambda_M(W) = \sum_{n=0}^{n_i} \chi_i^n(W) M^{ny} F_n[\chi_r(W)M^{1/\nu}] \quad (9)$$

and each F_n is again Taylor expanded up to order n_r

$$F_n = \sum_{m=0}^{n_r} F_{nm} \chi_r^m(W) M^{m/\nu}. \quad (10)$$

The nonlinearity in $\chi_r(W)$ and $\chi_i(W)$ is taken into consideration by series expansion in terms of $w = (W_C - W)/W_C$ up to orders m_r and m_i, respectively,

$$\chi_r(w) = \sum_{i=1}^{m_r} b_i w^i \quad \text{and} \quad \chi_i(w) = \sum_{j=0}^{m_i} c_j w^j \quad (11)$$

with $b_1 = c_0 = 1$. The total number of fit parameters, including ν, W_C, and y, is $N_p = (n_i+1)(n_r+1) + m_i + m_r + 2$. The Levenberg-Marquardt method is used to perform the nonlinear fit.[30] The quality of a fit is judged by the goodness-of-fit parameter Q,[30] which overall evaluates the least-mean-square value, χ^2, of Eq. (8), the number of data points, and fit parameters. Therefore, our criteria for choosing the correction terms is to assure a fast convergence in fitting functions and to maximize the goodness-of-fit Q while keeping the number of fitting parameters to a minimum.

TABLE I. The parameter settings for the three cases.

	Case 1	Case 2	Case 3
Δ	0.0	4.0	4.0
W_A	W	W	W
W_B	W	W	0.0
No. of bands	1	2	2

III. NUMERICAL RESULTS AND DISCUSSIONS

The complex lattice model presented in Sec. II suggests that it evolves smoothly from the usual one-band BCC simple lattice to the two-band complex lattice depending on the value of charge-transfer energy and on the disorder distribution. Three typical cases of this model are as follows: case 1: $\Delta=0$ and $W_A=W_B=W$, the disorder problem in BCC lattice; case 2: $\Delta\neq 0$ and $W_A=W_B=W$, uniform disorder in two-band complex lattice; and case 3: $\Delta\neq 0$, $W_A\neq 0$, and $W_B\equiv 0$, site-selective disorder in two-band complex lattice. The parameter setting of three cases is summarized in Table I. In order to guarantee meaningful fits to obtain reliable critical parameters, all $\Lambda_M(W)$s are calculated with a high accuracy of 0.1%. In addition, a generalized scaling function Eq. (8) is used to account for the contributions of both the relevant and irrelevant scaling variables, and the resulting scaling function f is obtained after subtracting the part from irrelevant scaling variable, which yields the critical disorder strength and the critical exponent.

For easy comparison with previous studies, we start our discussion with case 1. In Fig. 2, the reduced localization length $\Lambda_M(W)$, the scaling function $f[\xi(W)/M]$, and the scaling parameter $\xi(W)$ are plotted for various lateral sizes M and disorder strengths W at the band edge ($E=-8$). A critical disorder strength W_C is evident in Fig. 2(a) where $\Lambda_M(W)$ increases with M for extended states ($W<W_C$) and decreases with M for localized states ($W>W_C$). The drift in cross point at small M calls for the correction from irrelevant scaling variable and best fit parameters are summarized in Table II. From the corrected scaling function shown in Fig. 2(b), one finds that all $\Lambda_M(W)$s collapse almost perfectly onto a single curve after introducing the scaling parameter $\xi(W)$ plotted as inset. An MIT is clearly demonstrated by the two branches. The extracted critical exponent, $\nu=1.55\pm0.05$, and critical disorder strength, $W_C=21.79\pm0.04$, are in good agreement with recent calculation.[24] The localization length and scaling behavior have been extensively studied for the whole band, and all of them are quite similar to those shown in Fig. 2.

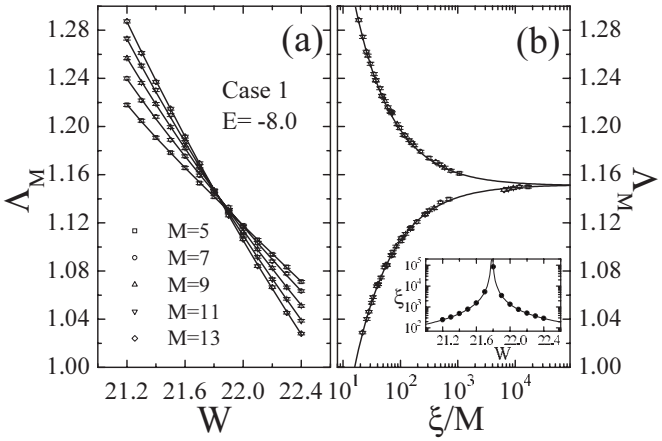

FIG. 2. The representative data for case 1 at $E=-8$. (a) $\Lambda_M(W)$ vs W and (b) $\Lambda_M(W)$ vs $\xi(W)/M$ with $\xi(W)$ shown as inset. The symbols with error bars are data points and the lines are fits using Eqs. (8)–(11).

The results for the other two typical energies ($E=0$, $E=-4.0$) are listed in Table II. The critical exponents all take a universal value within their error bars and are consistent with the previous result.[20,24]

Based on the same analysis, the energy-disorder phase diagram of case 1 is calculated and shown in Fig. 3. The overall shape of the phase diagram agrees very well with the recent study.[24] The critical disorder strength is symmetrical about the band center. It takes maximum values at the band edges of unperturbed band and takes a local minimum at the band center. Outside the unperturbed band ($|E|\geq 8$), the reentrance phenomenon appears due to the competition between quantum interference and quantum tunneling.[11] In comparison with that of SC lattice model, two notable features are worthy of mentioning. The critical disorder within the unperturbed band of BCC lattice is generally much larger than that of SC lattice, which may be attributed to the increased coordination number in BCC lattice. More nearest neighbors imply more hopping paths for electrons so that the stronger disorder is needed to localize electronic states. However, the weak W_C minimum at the band center seems to be a unique property for BCC lattice while a weak maximum occurs at the band center for SC lattice. The logarithmic singularity in DOS of BCC lattice may be responsible for this feature.

Now we continue our discussion to a two-band complex lattice with nonzero Δ. To be specific, we take $\Delta=4$ in the following. We first study case 2 with the uniform disorder on all lattice sites. Since the symmetry between the lower and

TABLE II. The best estimates of the critical disorder and critical exponent for case 1. The range of the lateral size M and the disorder strength W for the raw data, the form of fitting function (n_r, n_i, m_r, and m_i), the least-mean-square value χ^2, and the goodness-of-fit Q are listed.

E	W_C	ν	y	M	W	n_r	n_i	m_r	m_i	χ^2	Q
0.00	20.78 ± 0.02	1.54 ± 0.04	-3.1 ± 0.7	5–13	20.3–21.5	2	1	1	4	57.02	0.29
−4.00	21.04 ± 0.03	1.63 ± 0.07	-2.0 ± 0.5	5–13	20.6–21.8	2	1	4	2	65.09	0.10
−8.00	21.79 ± 0.04	1.55 ± 0.05	-2.2 ± 0.5	5–13	21.2–22.4	1	1	3	3	39.64	0.91

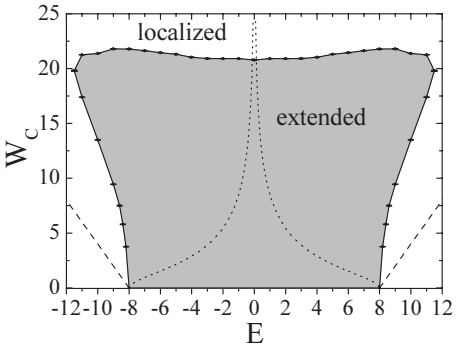

FIG. 3. The energy-disorder phase diagram for case 1. The symbols with error bars are data points. The extended and localized regions are marked as gray and white. The dotted line illustrates the unperturbed DOS and the dashed line sketches the border of DOS in the presence of disorder.

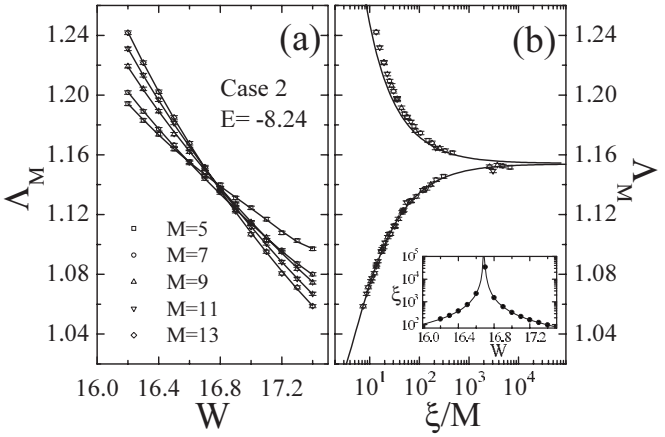

FIG. 4. Same as Fig. 2 but for case 2 at $E=-8.24$.

upper bands still holds for the localization properties, only results on the lower band are presented. The reduced localization lengths are calculated for various lateral sizes and disorder. The typical data of $\Lambda_M(W)$ at the lower edge of the lower band ($E=-8.24$) are presented in Fig. 4(a). The scaling function f and scaling parameter $\xi(W)$ are analyzed in the same way as before from the raw data and they are produced in Fig. 4(b) with the corresponding fitting parameters summarized in Table III. Figure 4 shows that an MIT occurs at critical disorder strength $W_C=16.69\pm0.05$. All the raw data fit nicely onto a common curve after subtracting the correction from the irrelevant scaling variable. The localization lengths calculated for the other band edge and band center all demonstrate similar scaling behaviors. The critical exponents, critical disorders as well as fitting parameters are summarized in Table III. Within the numerical accuracy the critical exponent in case 2 is consistent with that of the single-band lattice model since the universality class remains unchanged in the presence of charge-transfer energy Δ.

The comprehensive picture of localization property on case 2 can be visualized in the phase diagram shown in Fig. 5. Similarly to case 1, the critical disorder has a mirror-reflection symmetry about $E=0$. However, no mirror symmetry exists within the lower and upper bands individually. The shape of the phase diagram of case 2 differs significantly from that of case 1. The most notable change takes place near the edges of lower and upper bands. Unlike the slightly enhanced W_C shoulder at the outer edges for BCC lattice, the critical disorder strength is drastically depressed at the outer edges for complex lattice under uniform disorder. Furthermore, there is a small window of localized states within the band gap at low disorder strength. Thus, the reentrance phenomenon not only appears, as usual, outside the outer edges of both bands ($|E|>8.24$) but also appears between the two bands ($|E|<2$). The nonflat critical disorder within the unperturbed bands suggests that the localization mechanism is somewhat different for cases of simple lattice and complex lattice. The possible reason might be related to the induced intraband off-diagonal disorder. It is well known that the off-diagonal disorder can make the critical disorder energy dependent.[21]

Among the three cases we have investigated in this paper, case 3 with site-selective disorder turns out to be the most interesting since it can simulate more realistic situation for doping in mixed valence compounds. The site-selective disorder in the A sublattice has stronger scattering effect on lower band than on upper band, which is fully confirmed by our numerical calculations. In Fig. 6(a), the raw data for reduced localization lengths $\Lambda_M(W)$ is displayed for the electronic state at the lower edge of lower band ($E=-8.24$) and a metal-insulator transition is evident. The derived single parameter scaling function is shown in Fig. 6(b) with the scaling parameter plotted as inset. The critical disorder strength is $W_C=14.37\pm0.01$ and critical exponent is $\nu=1.64\pm0.02$. Other fitting parameters are included in Table IV. Since the scaling property on other energies of the lower band shows a similar behavior, only the critical parameters are listed in Table IV. Generally speaking, W_C decreases from the upper edge to lower edge for the low band, and the critical exponent remains universal within the numerical accuracy.

An interesting feature reflecting the weak disorder effect on the upper band is the presence of a unique type of delocalized state at the lower edge of the upper band ($E=2$). To see what happens at this particular energy, the localization lengths are calculated as a function of the layer number L. Unlike the localization length $\lambda_M(W)$ computed for other states in the lower and upper bands with $E\neq2$ where con-

TABLE III. Same as Table II but for case 2.

E	W_C	ν	y	M	W	n_r	n_i	m_r	m_i	χ^2	Q
−2.00	20.80 ± 0.04	1.58 ± 0.07	−2.3 ± 0.6	5–13	20.3–21.5	3	1	2	0	62.22	0.18
−5.00	21.10 ± 0.03	1.59 ± 0.04	−3.4 ± 0.6	5–13	20.6–21.8	2	1	2	4	43.73	0.76
−8.24	16.69 ± 0.05	1.47 ± 0.08	−2.8 ± 0.8	5–13	16.2–17.4	2	2	3	3	42.17	0.71

TABLE IV. Same as Table II but for case 3.

E	W_C	ν	y	M	W	n_r	n_i	m_r	m_i	χ^2	Q
8.24	23.59 ± 0.01	1.61 ± 0.02	-2.1 ± 0.8	5–13	22.9–24.1	2	1	2	2	59.92	0.24
5.00	35.32 ± 0.01	1.52 ± 0.05		5–13	34.7–35.9	4	0	2	0	68.93	0.13
−2.00	21.23 ± 0.02	1.66 ± 0.06	-2.9 ± 0.7	5–13	20.5–21.7	2	1	4	0	58.43	0.28
−5.00	15.14 ± 0.01	1.59 ± 0.04		5–13	14.5–15.7	4	0	3	0	66.72	0.15
−8.24	14.37 ± 0.01	1.64 ± 0.02	-3.2 ± 0.6	5–13	13.8–15.0	3	1	2	1	53.56	0.41

vergent values are always reached, $\lambda_M(W)$ ($\approx 1.47666 \times 10^6 + 0.04483 \times L$) at $E=2$ collapses to a single common curve up to the largest layer number $L=2\times10^9$ the computer can handle. The localization lengths neither depend on M nor depend on W. The relative errors among different sets are estimated to be less than 10^{-4}. Also $\lambda_M(W)$ is very large (10^7) in comparison with the lateral size. It is roughly six orders of magnitude larger than those calculated for all other cases. The linear dependence of $\lambda_M(W)$ on L suggests that the state at the lower band edge can be classified as a delocalized state along the propagation direction. This delocalized state is similar to the state at the band center in 3D SC lattice model[21,22] and two-dimensional (2D) square lattice model[23] in the presence of purely off-diagonal disorder. In 3D SC lattice the delocalized state is dependent on lateral size M and is independent of the disorder strength while in 2D square lattice the critical state depends both on lateral size M and the disorder strength. The detailed analytic analysis shows that the wave function amplitudes in sublattice A and sublattice B are decoupled at $E=2$, and all eigenstates retain finite amplitudes only in sublattice B while they are identically zeros in sublattice A. This is the reason why the localization length $\lambda_M(W)$ depends neither on disorder strength W nor on lateral size M.

Except the states at $E=2$, $\Lambda_M(W)$ shows a common pattern of 3D disordered systems for all other energies of upper band. The results on the band center and upper band edge are listed in Table IV for easy comparison. W_C decreases with increasing band energy and the critical exponent takes more or less the same value. In comparison with previous studies,[20,24] our lattice model shows that the site-selective disorder does affect the critical disorder unevenly for the upper and lower bands. It even introduces the delocalized states at the lower edge of less disorder-affected band but the universality class of the system remains intact.

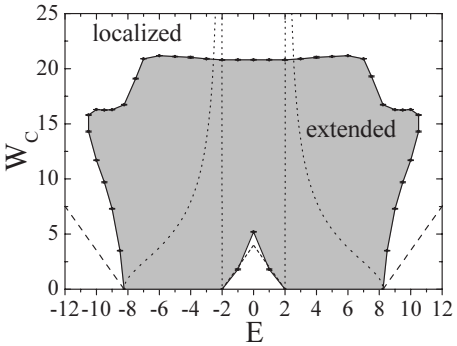

FIG. 5. Same as Fig. 3 but for case 2.

The phase diagram for case 3 is shown in Fig. 7. Two interesting features are worthy of mentioning: (1) the site-selective disorder breaks the mirror symmetry between the lower and upper bands, and the states in the upper band are more delocalized than those of lower band and (2) the singular form of W_C near the lower edge of upper band indicates the energy region where the states are most difficult to be localized. The asymmetrical phase diagram might be used for purposed doping which introduces the required carriers but without sacrificing significantly the mobility of the carriers.

IV. CONCLUSION

In conclusion, the reduced localization lengths, scaling function, scaling parameter $\xi(W)$, and critical parameters are calculated for CsCl-type complex Anderson lattice model using the transfer-matrix method and finite-size scaling. The values of the critical exponent ν are in good agreement with those obtained previously for other simple lattices belonging to the orthogonal class. For all band energies except that at the lower edge of the upper band, there exists MIT. The raw data can be fitted into a common scaling curve, validating the single-parameter scaling theory in the two-band lattice model. For site-selective disorder, an asymmetric localization behavior is observed among the two bands. Furthermore, a unique type of delocalized state is found at the lower edge of the less disorder-affected band. The calculated localization length increases monotonically with sample size but is independent of the lateral size M and disorder strength W. The complex Anderson lattice model with site-selective dis-

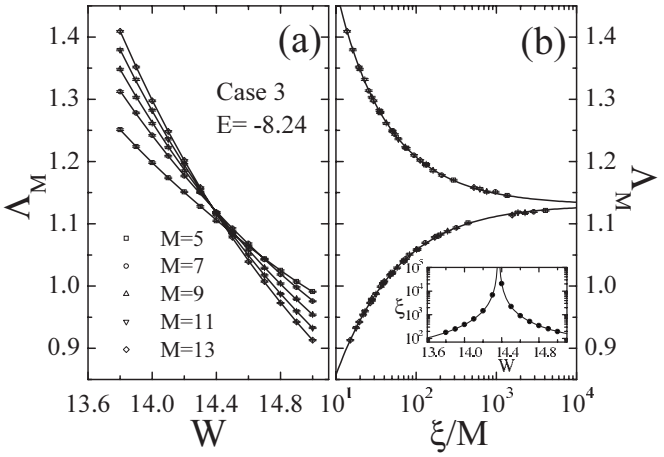

FIG. 6. Same as Fig. 2 but for case 3 at $E=-8.24$.

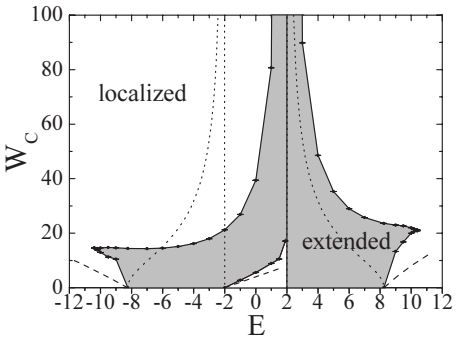

FIG. 7. Same as Fig. 3 but for case 3. The vertical solid line at $E=2$ represents a unique type of delocalized state.

order naturally explains the asymmetrical properties between the lower and upper bands, which is relevant to the asymmetrical localization behavior between electron- and hole-doped compounds.

ACKNOWLEDGMENTS

This work was supported in part by the National Basic Research Program of China (Grant Nos. 2007CB925104 and 2010CB923404). We wish to acknowledge the partial financial support from the NNSFC under Grant No. 10774066 and "Excellent Youth Foundation" (Grant No. 10025419).

[1] P. W. Anderson, Phys. Rev. **109**, 1492 (1958).
[2] D. J. Thouless, Phys. Rep. **13**, 93 (1974).
[3] E. Abrahams, P. W. Anderson, D. C. Licciardello, and T. V. Ramakrishnan, Phys. Rev. Lett. **42**, 673 (1979).
[4] G. Bergmann, Phys. Rep. **107**, 1 (1984).
[5] B. Kramer and A. MacKinnon, Rep. Prog. Phys. **56**, 1469 (1993).
[6] J. L. Pichard and G. Sarma, J. Phys. C **14**, L127 (1981).
[7] A. D. Zdetsis, C. M. Soukoulis, E. N. Economou, and Gary S. Grest, Phys. Rev. B **32**, 7811 (1985).
[8] A. MacKinnon, J. Phys. Condens. Matter **6**, 2511 (1994).
[9] A. MacKinnon and B. Kramer, Phys. Rev. Lett. **47**, 1546 (1981).
[10] A. MacKinnon and B. Kramer, Z. Phys. B: Condens. Matter **53**, 1 (1983).
[11] B. R. Bulka, B. Kramer, and A. MacKinnon, Z. Phys. B: Condens. Matter **60**, 13 (1985).
[12] B. R. Bulka, M. Schreiber, and B. Kramer, Z. Phys. B: Condens. Matter **66**, 21 (1987).
[13] B. Kramer, K. Broderix, A. MacKinnon, and M. Schreiber, Physica A **167**, 163 (1990).
[14] I. Kh. Zharekeshev and B. Kramer, Phys. Rev. B **51**, 17239 (1995).
[15] H. Grussbach and M. Schreiber, Phys. Rev. B **51**, 663 (1995).
[16] H. Stupp, M. Hornung, M. Lakner, O. Madel, and H. v. Löhneysen, Phys. Rev. Lett. **71**, 2634 (1993).
[17] K. M. Itoh, E. E. Haller, J. W. Beeman, W. L. Hansen, J. Emes, L. A. Reichertz, E. Kreysa, T. Shutt, A. Cummings, W. Stockwell, B. Sadoulet, J. Muto, J. W. Farmer, and V. I. Ozhogin, Phys. Rev. Lett. **77**, 4058 (1996).
[18] S. Waffenschmidt, C. Pfleiderer, and H. v. Löhneysen, Phys. Rev. Lett. **83**, 3005 (1999).
[19] K. M. Itoh, M. Watanabe, Y. Ootuka, and E. E. Haller, Ann. Phys. (Leipzig) **8**, 631 (1999).
[20] K. Slevin and T. Ohtsuki, Phys. Rev. Lett. **82**, 382 (1999).
[21] P. Cain, R. A. Römer, and M. Schreiber, Ann. Phys. (Leipzig) **8**, SI-33 (1999).
[22] M. Fabrizio and C. Castellani, Nucl. Phys. B **583**, 542 (2000).
[23] A. Eilmes, R. A. Römer, and M. Schreiber, Eur. Phys. J. B **1**, 29 (1998).
[24] A. Eilmes, A. M. Fischer, and R. A. Römer, Phys. Rev. B **77**, 245117 (2008).
[25] I. V. Plyushchay, R. A. Römer, and M. Schreiber, Phys. Rev. B **68**, 064201 (2003).
[26] R. J. Jelitto, J. Phys. Chem. Solids **30**, 609 (1969).
[27] D. Klotsa, R. A. Römer, and M. S. Turner, Biophys. J. **89**, 2187 (2005).
[28] C. J. Lambert and D. Weaire, Phys. Status Solidi B **101**, 591 (1980).
[29] V. I. Oseledec, Trans. Mosc. Math. Soc. **19**, 197 (1968).
[30] W. H. Press, B. P. Flannery, S. A. Teukolsky, and W. T. Vetterling, *Numerical Recipes in FORTRAN*, 2nd ed. (Cambridge University Press, Cambridge, 1992).